Scaling characteristics of hilltop and hilltop-squared inflation

Monika Lynker* and Rolf Schimmrigk†
Department of Physics, Indiana University South Bend,
1700 Mishawaka Avenue, South Bend, Indiana 46615, USA

(Received 28 December 2023; accepted 29 May 2024; published 9 July 2024)

One of the long-standing goals in the framework of inflation is the construction of tools that can be used to classify models in theory space. An idea that has been put forward in this context is to consider the energy-dependent scaling behavior of observables to characterize different models. We implement this approach in the framework of hilltop and hilltop-squared inflation by analyzing their observables when the small-field approximation is not imposed and the energy scale μ of these models is varied as a free parameter, subject to observational constraints. We show that the scalar spectral tilt and the tensor ratio r exhibit μ-dependent scaling behavior and that the scaling exponents as functions of μ in turn lead to functional forms that are model dependent. Scaling relations of the type discussed here are of interest as characteristics of the inflationary theory space as well as in the context of the postinflationary reheating process. We further observe a bifurcation behavior in the behavior of p-families in the spectral-tensor plane for a critical value of μ.

DOI: 10.1103/PhysRevD.110.023508

I. INTRODUCTION

Hilltop-type potentials have remained among the canonical models of inflation. While the general class of hilltop theories encompasses a wide variety of potentials that have been discussed in the context of a number of embedding theories (see, e.g., the reviews [1,2] for many references), our focus here is on a more specific set of models, defined as

$$V_{p,n} = \Lambda^4\left(1 - \left(\frac{\phi}{\mu}\right)^p\right)^n, \tag{1}$$

where $n = 1, 2$. Some of the models in this class have become benchmark models for the cosmic microwave background (CMB) collaborations [3–8]. While hilltop models, in general, and the $V_{p,n}$ above, in particular, have traditionally been considered in the context of single-field inflation (see, e.g., [2,9–35]), this class of potentials is also of interest in the framework of multifield inflationary models that describe saddle point inflation. In this context, hilltop potentials can be used as single-field approximations of inflaton trajectories that roughly evolve along a cross section in the concave direction of the multifield potentials. Examples of this latter type include the models of j inflation and h inflation in the framework of modular inflation [36–41].

The potentials $V_{p,n}$ describe two-parameter single-field inflationary models and as such are amenable to the scaling-type analysis that was introduced in Ref. [42] in the context of multifield inflation. In was observed there that theories with two parameters may lend themselves to a characterization in terms of a family of scaling relations with associated scaling exponents β_p that are specific to the models and therefore could be used to distinguish regions in the inflationary theory space. Furthermore, if the exponents β_p are functions $\beta_p(\mu)$ of the energy scale μ, one can ask whether they in turn show scaling behavior with an associated exponent γ_p that would then provide a single number associated with the parameter space of the model. Such scaling relations were established in [42] in the context of modular inflation, which is a class of two-field models. The same question can be raised in the context of other models with two parameters and, in the present analysis, we focus on hilltop-type potentials. We vary the exponent p in $V_{p,n}$ systematically and consider the dependence of the observables on the energy scale μ. We will focus on pure slow-roll inflation, without making any further approximations that were adopted in early papers on these models. Making such additional approximations eliminates the dependence of the observables on the energy and thereby trivializes the scaling behavior. Imposing such approximations implies, for example, that the critical exponent of the tensor ratio is energy independent, hence there is no functional dependence of the scaling exponents on μ.

Depending on the exponent n in (1) the models exhibit a quite different structure close to the minimum at $\phi = \mu$. While hilltop inflation ($n = 1$) intersects the zero line with a nonzero slope, hilltop-squared models have a smooth valley around the minimum. The fact that there is no valley

*mlynker@iu.edu
†rschimmr@iu.edu, netahu@yahoo.com

for the hilltop models has sometimes been considered a weakness of these models because, strictly speaking, this means that these models do not have a domain that allows the inflaton to oscillate around the minimum, thereby releasing its energy to other particles whose couplings to the inflaton are assumed to be small and negligible during inflation but become relevant during the postinflation process of reheating. As a practical matter this issue can be resolved by simply gluing an appropriate potential to $V(\phi_e)$ for $\phi > \phi_e$ to the hilltop potential. The fact that this issue does not arise for hilltop-squared theories has been a motivation to consider these models, see, e.g., [7,32,34,35]. Discussions concerning the embedding of hilltop models in fundamental theories can be found, for example, in the work of [43–45] and references cited therein.

We have organized this paper as follows. Section II describes the observables we will focus on in both the pure slow-roll and in their different small-field approximations. In Sec. III we briefly consider the reheating constraint so as to be able to gauge its effect when imposed in addition to the CMB constraints. In Sec. IV we present the impact of the CMB and reheating constraints for the class of hilltop models and in Sec. V we discuss the scaling distributions that will be made quantitative for hilltop models in Sec. VI. In Sec. VII we analyze p-families of hilltop models in dependence of the energy scale μ and describe a bifurcation phenomenon that appears at a critical value of this scale. In Sec. VIII we extend our analysis to the hilltop-squared models and in Sec. IX we discuss the implications of our scaling analysis as a tool that provides characteristic quantities defined on the inflationary landscape. We conclude in Sec. X.

II. OBSERVABLES IN HILLTOP INFLATION

Our focus in this work is on hilltop inflation in the pure slow-roll approximation, but it is of interest to compare our results with the behavior of this class of models in the small-field approximation. We discuss these approximations in turn.

A. Slow-roll approximation

The analysis in the following is concerned with the observables at horizon crossing as functions of the inflaton ϕ_* and the number of e-folds N_* between horizon crossing time t_* and the end of inflation t_e. For the Lukash-Bardeen perturbation [46–48]

$$\mathcal{R} = H\delta u - \psi, \tag{2}$$

where $H = \dot{a}/a$ is the Hubble-Slipher parameter, ψ is the metric potential, and δu is obtained from δT_{0i}, the spectral index and the tensor-to-scalar ratio take the form

$$n_{\mathcal{R}\mathcal{R}} = 1 - p\frac{M_{\rm Pl}^2}{\mu^2}\frac{(\frac{\phi}{\mu})^{p-2}}{(1-(\frac{\phi}{\mu})^p)^2}\left[2(p-1)+(p+2)\left(\frac{\phi}{\mu}\right)^p\right].$$
$$r = 8p^2\frac{M_{\rm Pl}^2}{\mu^2}\frac{(\frac{\phi}{\mu})^{2(p-1)}}{(1-(\frac{\phi}{\mu})^p)^2}, \tag{3}$$

while the number of e-folds is given by

$$N_* = \frac{\mu^2}{pM_{\rm Pl}^2}\left[\frac{1}{p-2}\left(\left(\frac{\mu}{\phi_*}\right)^{p-2}-\left(\frac{\mu}{\phi_e}\right)^{p-2}\right) - \frac{1}{2}\left(\left(\frac{\phi_e}{\mu}\right)^2-\left(\frac{\phi_*}{\mu}\right)^2\right)\right]. \tag{4}$$

The end-of-inflation value ϕ_e will be determined by the constraint $\epsilon_V(\phi_e) = 1$, which is obtained from the constraint

$$\left(\frac{\phi_e}{\mu}\right)^p + \frac{p}{\sqrt{2}}\frac{M_{\rm Pl}}{\mu}\left(\frac{\phi_e}{\mu}\right)^{p-1} - 1 = 0. \tag{5}$$

We will use two different ways to analyze these models phenomenologically. The first is the "scan method," in which the strategy is to systematically scan the parameter space (Λ, μ, ϕ_*) for viable models within the available constraints, in particular, the CMB results for $n_{\mathcal{R}\mathcal{R}}, r$ from PLANCK as well as the adopted range for the number of e-folds. This is in the spirit of earlier analyses in a different context, such as [41]. The second is the "p-family method," where the idea is to choose a fixed number of e-folds N, say $N = 60$, and determine ϕ_* in terms of N_*, where ϕ_e has been solved via $\epsilon_V(\phi_e) = 1$, as usual. Having determined $\phi_*(N)$ by inverting the $N_\star$ equation in (4) leads to

$$\left(\frac{\phi_*}{\mu}\right)^p - A_p\left(\frac{\phi_*}{\mu}\right)^{p-2} + \frac{2}{p-2} = 0 \tag{6}$$

with

$$A_p := 2p\frac{M_{\rm Pl}^2}{\mu^2}N_* + \left(\frac{\phi_e}{\mu}\right)^2 + \frac{2}{p-2}\left(\frac{\mu}{\phi_e}\right)^{p-2}. \tag{7}$$

In this way, one can compute the observables for a given μ. This method was considered, for example, in the early hilltop papers [9,10] (see also [21]).

B. Small-field approximations of hilltop inflation

The small-field approximation can be implemented in different forms. The weakest form requires only that the initial value ϕ_* is much smaller than the energy scale μ. More interesting is the stronger approximation that ϕ is much smaller than μ throughout inflation, because this allows one to obtain analytical expressions for the observables. While consistency with the model does place

restrictions on μ, these are model dependent and are weaker than the sub-Planckian constraint often encountered as part of the small-field definition. In order to distinguish these different approximations, we use the designations SF.I for the weakest version, SF.II for the version that covers all of inflation, and SF.III for the version that furthermore imposes an *a priori* constraint on the energy scale μ that is model-independent.

The motivation for SF.II comes from the fact that, in this case, one can use the resulting e-fold formula

$$N_* = \frac{\mu^2}{p(p-2)M_{\rm Pl}^2}\left(\left(\frac{\mu}{\phi_*}\right)^{p-2} - \left(\frac{\mu}{\phi_e}\right)^{p-2}\right) \tag{8}$$

to solve analytically for ϕ_* as a function of N_*. Using this solution, we can write the e-fold dependence of the spectral index as

$$n_{\mathcal{RR}}(p,\mu,N_*) = 1 - \frac{2(p-1)}{(p-2)N_* + \frac{1}{p}\left(\frac{p}{\sqrt{2}}\right)^{(p-2)/(p-1)}\left(\frac{\mu}{M_{\rm Pl}}\right)^{p/(p-1)}} \tag{9}$$

and the tensor-to-scalar ratio as

$$r(N_*,\mu,p) = \frac{8p^2\left(\frac{\mu}{M_{\rm Pl}}\right)^{2p/(p-2)}}{\left(p(p-2)N_* + \left(\frac{\mu}{M_{\rm Pl}}\right)^{p/(p-1)}\left(\frac{p}{\sqrt{2}}\right)^{(p-2)/(p-1)}\right)^{2(p-1)/(p-2)}}. \tag{10}$$

This μ-dependent form of the small-field approximation does not lead to an analytical N_*-scaling relation for either of the observables, which is presumably why it has not been considered in the literature. However, we can think of these expressions as functions that indicate a kind of "effective" scaling relation with energy-dependent exponents and amplitudes. This point will turn out to be useful later in this paper to gain a qualitative understanding of the μ dependence of hilltop inflation.

While neither r nor $n_{\mathcal{RR}}$ scale with N_* directly in the SF.II approximation, the tensor ratio does scale analytically with the spectral tilt $\delta_n = 1 - n_{\mathcal{RR}}$ as

$$r(n_{\mathcal{RR}},\mu) = \frac{8p^2\left(\frac{\mu}{M_{\rm Pl}}\right)^{2p/(p-2)}}{(2p(p-1))^{2(p-1)/(p-2)}}\delta_n^{2(p-1)/(p-2)}. \tag{11}$$

This shows that even in the SF.II approximation the tensor ratio varies for the class of hilltop models and that typicality statements made in the literature about the behavior of the tensor ratio as a function of $n_{\mathcal{RR}}$ do not apply in general. The slow-roll form of this relation will be discussed in Sec. IV.

Our results below will show that, while the SF.II approximation does capture qualitatively certain features of hilltop inflation, it is only a good approximation in a limited parameter range that is not enforced by observations. Furthermore, while in some parameter regions the small-field approximation might be reasonable at the beginning of hilltop inflation it is, in general, less so toward the end of inflation. If the μ-terms in the denominators are neglected, the spectral index reduces in the resulting SF.III approximation to the μ-independent spectral index

$$n_{\mathcal{RR}}(p,N_*) = 1 - \frac{2(p-1)}{(p-2)}\frac{1}{N_*} \tag{12}$$

considered in the early hilltop papers [9,10]. Similarly, in this limit the tensor ratio reduces to the form discussed in [11]

$$r(N_*) = 8p^2\left(\frac{\mu}{M_{\rm Pl}}\right)^{2p/(p-2)}\frac{1}{(p(p-2)N_*)^{2(p-1)/(p-2)}}. \tag{13}$$

In both relations the exponents are independent of the energy, which is not the case in the slow-roll or the small-field approximation SF.II.

III. REHEATING CONSTRAINT

While our main focus is in the energy dependence of the scaling behavior in hilltop and hilltop-squared inflation, it is of interest to see how the reheating constraints affect the distributions associated with the initial conditions of the inflaton field. For this we consider the usual insertion of phases between horizon crossing and today, in combination with the evolution of the energy density during reheating and the conservation of entropy between the end of reheating and today. The simplest analyses assume that the equation of state parameter $w_{\rm rh}$ is constant, so that

$$\rho_{\rm rh} = \rho_e\left(\frac{a_e}{a}\right)^{3(1+w_{\rm rh})}, \tag{14}$$

an assumption that is made in much of the literature. The detailed form of the phase evolution analysis of the scale factor depends on how the expansion of the k_*/k_0 is done, but the end result is essentially the same, see, for example, [49–53]. For our purpose, it is useful to evaluate the resulting formula for the e-folds $N_{\rm rh}$ during reheating for potentials of the type $V = \Lambda^4 f(\phi/\mu)$, where f is a dimensionless function. The overall energy scale Λ is determined by the CMB amplitude $\mathcal{A}_{\mathcal{R}}$, leading to

$$N_{\rm rh} = \frac{4}{1-3w_{\rm rh}}\left(-N_* + \frac{1}{4}\ln\frac{(f'_*)^2}{f_* f_e} + \frac{1}{2}\ln\frac{M_{\rm Pl}}{\mu} + \sigma_{\rm piv}\right), \tag{15}$$

where f_* is the dimensionless potential evaluated at ϕ_*, f_e is its value at the end of inflation, and f' is the

dimensionless derivative of f. The parameter $\sigma_{\rm piv}$ is a model-independent constant

$$\sigma_{\rm piv} = \ln\frac{a_0 T_0}{k_*} - \frac{1}{3}\ln\frac{11 g_{\rm rh}}{43} - \frac{1}{4}\ln\frac{405}{\pi^2 g_{\rm rh}} + \frac{1}{4}\ln(12\pi^2\mathcal{A}_{\mathcal{R}}), \tag{16}$$

determined by the CMB amplitude $\mathcal{A}_{\mathcal{R}}$ and the pivot scale k_*, as well as $g_{\rm rh}$ and T_0. For the reheating temperature, we obtain in terms of the dimensionless potential f

$$T_{\rm rh} = M_{\rm Pl}\left(\frac{540}{g_{\rm rh}}\frac{M_{\rm Pl}^2}{\mu^2}\mathcal{A}_{\mathcal{R}}\frac{(f'_*)^2 f_e}{f_*^3}\right)^{1/4} e^{-\frac{3}{4}(1+w_{\rm rh})N_{\rm rh}}. \tag{17}$$

This compact form is convenient for computations even though it is written in a slightly redundant form. The energy-dependent scaling relations obtained below for the observables lead to scaling behavior of $N_{\rm rh}$ and $T_{\rm rh}$ in dependence of these variables.

IV. SCALING BEHAVIOR OF HILLTOP INFLATION

Hilltop inflation has mostly been analyzed at low p and low μ. The model at $p = 4$, in particular, has been discussed often in the literature, see, e.g., [2,9–12,24–26,29,30,32,33], and has been adopted as a benchmark model by the CMB collaborations (see, e.g., [3,4,6–8]). In this section we investigate the impact of the CMB and reheating constraints more generally for these models and, in particular, analyze the behavior of the observables as the energy parameter μ is varied, similar to the analysis in [42] in the context of multifield inflation. The resulting data will be used in later sections for the scaling analyses.

We vary p through a wide set of models, ranging from 3 to 100, and for each p consider a range of μ values that is compatible with the CMB constraints on the spectral index $n_{\mathcal{RR}}$ and the tensor-to-scalar ratio r and also lead to sufficient inflation $N_* \in [50, 70]$. This μ range increases as p gets larger, both in the sub-Planckian and the super-Planckian regime. For low p, in particular, the models are not consistent with the CMB and e-fold constraints for sub-Planckian values for μ, but these become viable as p increases. We scan the complete μ range for super-Planckian values in an integral parametrization $\mu = mM_{\rm Pl}$, m an integer, and impose for larger p the generic p-independent lower bound $\mu = 10^{-2}M_{\rm Pl}$ for the sub-Planckian range. This lower bound is sufficient to indicate the behavior of these models, in particular, toward the low end of the tensor ratio that is probed by such μ values. The parametrization of these sub-Planckian ranges is via rational values $\mu = M_{\rm Pl}/m$. The upper bound on μ grows linearly with p with a slope of slightly less than 8, while the full sub-Planckian regime reaches for large p far below the Planck scale. While there is a weak correlation between the number of inflationary e-folds and μ, there is quite some degeneracy even for low p and this degeneracy increases for larger p. For the purpose of our discussion, a full scan of μ range is not necessary.

In Fig. 1 we illustrate the distributions mapped out by viable initial conditions in the spectral-tensor plane considered by the experimental collaborations. We adopt the values $n_{\mathcal{RR}} \in [0.96, 0.97]$ and $r_* \leq 0.035$, as suggested by the CMB experiments [8]. The color coding is blue for super-Planckian μ range and pure inflationary constraints, while red indicates the results after taking into account the reheating constraint $N_{\rm rh}$, which is implemented here for illustration with $w_{\rm rh} = 0$. Black is for μ in the sub-Planckian range with inflationary constraints and yellow indicates the inclusion of the reheating constraint. The first panel in Fig. 1 shows that the quartic hilltop model has no viable initial values for sub-Planckian μ values, which also holds for $p = 3$. The ranges of the inflaton field in both models are such that these models are no longer small-field inflation, given the current observational constraints. As p increases sub-Planckian energy values become possible and the viable μ bounds extend both in the sub- and the super-Planckian regime, leading to the regions in the parameter space in which these models can describe small-field inflation.

The overall shapes of the viable regions in the spectral-tensor plane of Fig. 1 are determined by a combination of constraints. The upper and lower boundary curves of the distributions come from the lower and upper bound of the number of inflationary e-folds. A smaller interval of allowed values N_* would lead to regions that are more narrow. The flat plateaus of the upper regions of the distributions in Fig. 1 show that the PLANCK bound on r constrains these models for all p. Future experiments like the Simons Observatory [5], CMB-S4 [6,7] and LiteBird [54] aim to reach $r \cong 0.001$ and will put more pressure on some of these models if gravitational waves are not found. In particular, the often considered quartic model could be excluded and the same applies even more to the cubic hilltop model because its lower bound of r is higher than for the quartic model. For larger p none of the upcoming CMB experiments will be able to exclude these models based on their target values of r in the range of a milli, even if the energy scale μ is restricted to super-Planckian values.

The results in Fig. 1 also show that for low p hilltop models improved constraints for the spectral index alone have the potential to significantly reduce the viable region in the spectral-tensor plane, while for higher p such constraints will have less impact since for larger p the region in these graphs covers the whole range of the spectral index, at least in the tensor ratio range considered here for sub-Planckian energy scales μ. This pattern is stable when p is increased to $p > 20$ as far as the CMB constraints above are concerned. Including the reheating constraint does not change the viable range of $n_{\mathcal{RR}}$ but does decrease the regions dramatically by its effect on the tensor

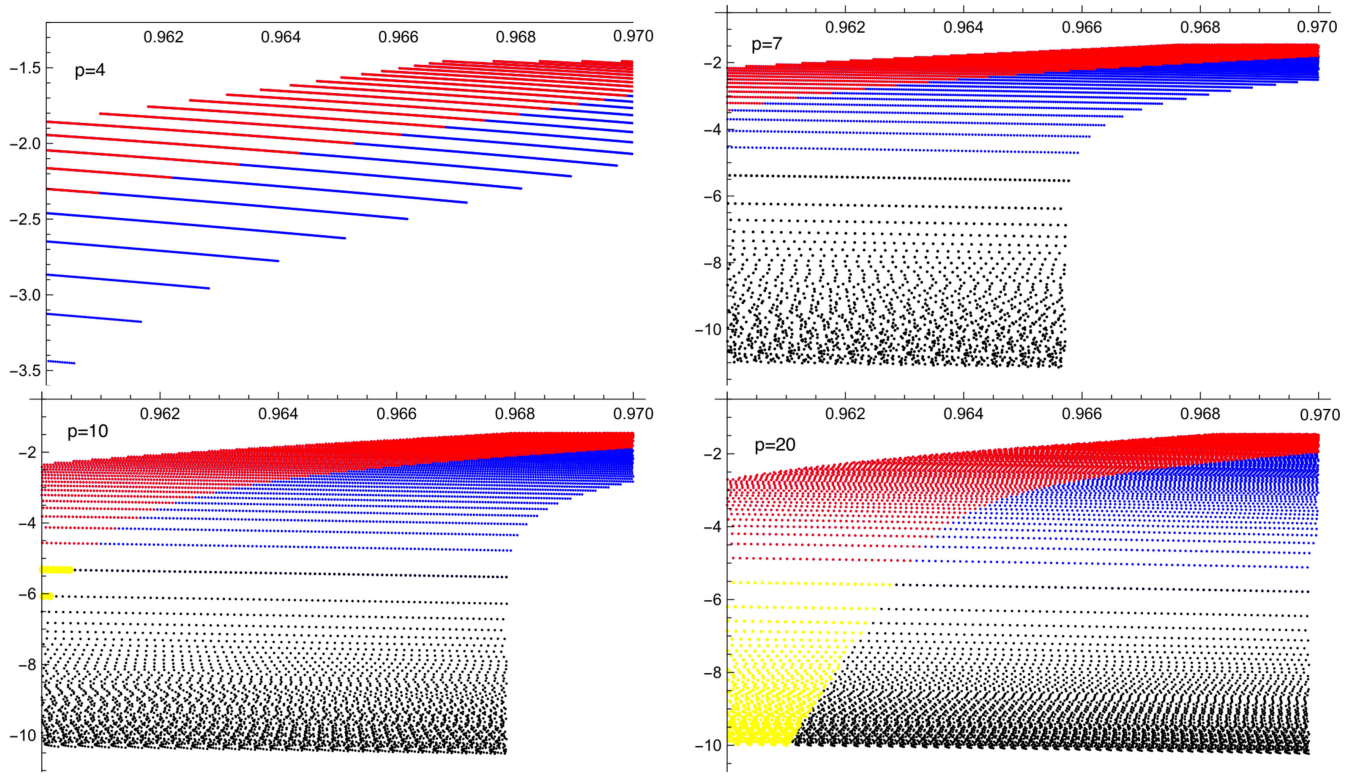

FIG. 1. The $(n_{\mathcal{RR}}, \log r)$ distributions for $p = 4, 7, 10, 20$ in the panels from the upper left to the lower right, respectively. Here the colors blue (red) indicate the super-Planckian μ without (with) the reheating constraint, while black (yellow) shows sub-Planckian domains without (with) the reheating constraint.

ratio. An improved accuracy of the spectral index $n_{\mathcal{RR}}$ could again limit the viability of this class of models with a matter dominated reheating phase. The combination of the results of the PLANCK probe with the upcoming large scale survey data, such as Euclid and SKA, will therefore have a significant impact on the hilltop models. A discussion of the uncertainties of different combinations of these three experiments is, for example, given in Ref. [55].

The μ-stratifications of Fig. 1 show that in hilltop inflation the tensor-to-scalar ratio r follows scaling relations in dependence of $n_{\mathcal{RR}}$ and that the scaling parameters vary as the energy scale μ is varied. This will be analyzed quantitatively in later sections by extending and generalizing the strategy adopted in the context of multifield inflation in Ref. [42]. Here we point to the fact that this energy dependence generalizes and refines assumptions made in the literature that neglect a possible variation of the amplitude and the exponents in the scaling relation [56,57]. These results make explicit the difference between the strong small-field approximation discussed earlier in this paper and the slow-roll approximation. In the former the scaling exponents are energy-independent, while Fig. 1 illustrates the significant variation of these parameters over the viable parameter space. As a result of this energy dependence the parameter spaces of the different hilltop models are constrained to a different degree, depending on p. The $(r, n_{\mathcal{RR}})$-scaling relations of Fig. 1 can be viewed as a consequence of the energy-dependent scaling relations of the spectral tilt $\delta_n(N)$ and the tensor ratio $r(N)$ as functions of the number of inflationary e-folds, which will be discussed in the next section.

The μ-stratification of the spectral-tensor plane also establishes correlations between some observables and the energy parameter that defines the deformation of the model. These are of different strength in that the correlation, for example, between the energy μ and the tensor ratio is quite strong, while the correlation between μ and the spectral index is much weaker. Other correlations, such as the anticorrelation between the number of inflationary e-folds N_* and the reheating e-folds $N_{\rm rh}$ depend on the model, becoming weaker as p increases. The bounds on these e-folds are, however, stable and lead to upper bounds of about 40 and about 60 for the reheating e-folds and the inflationary e-folds, respectively.

V. SCALING DISTRIBUTIONS IN HILLTOP INFLATION VIA N_*

Scaling functions in dependence of the model parameters can be used as characteristics of the inflationary theory space, as discussed in the context of multifield theories in [42]. While this is a particularly interesting tool in multifield models with nontrivial potentials, even single-field inflationary theories are usually not solvable analytically.

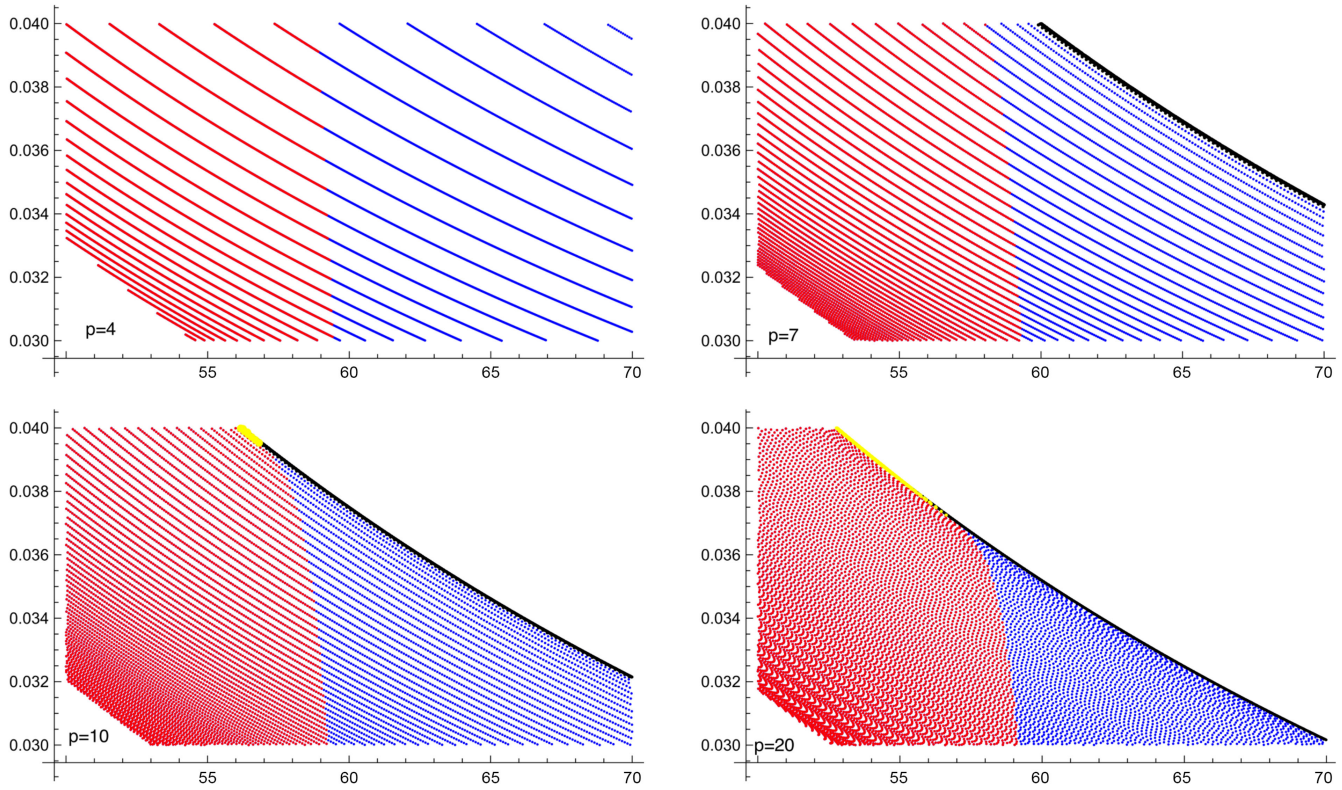

FIG. 2. Scaling distributions for (N_*, δ_n) in hilltop inflationary models with $p = 4, 7, 10, 20$. The color scheme is the same as in Fig. 1.

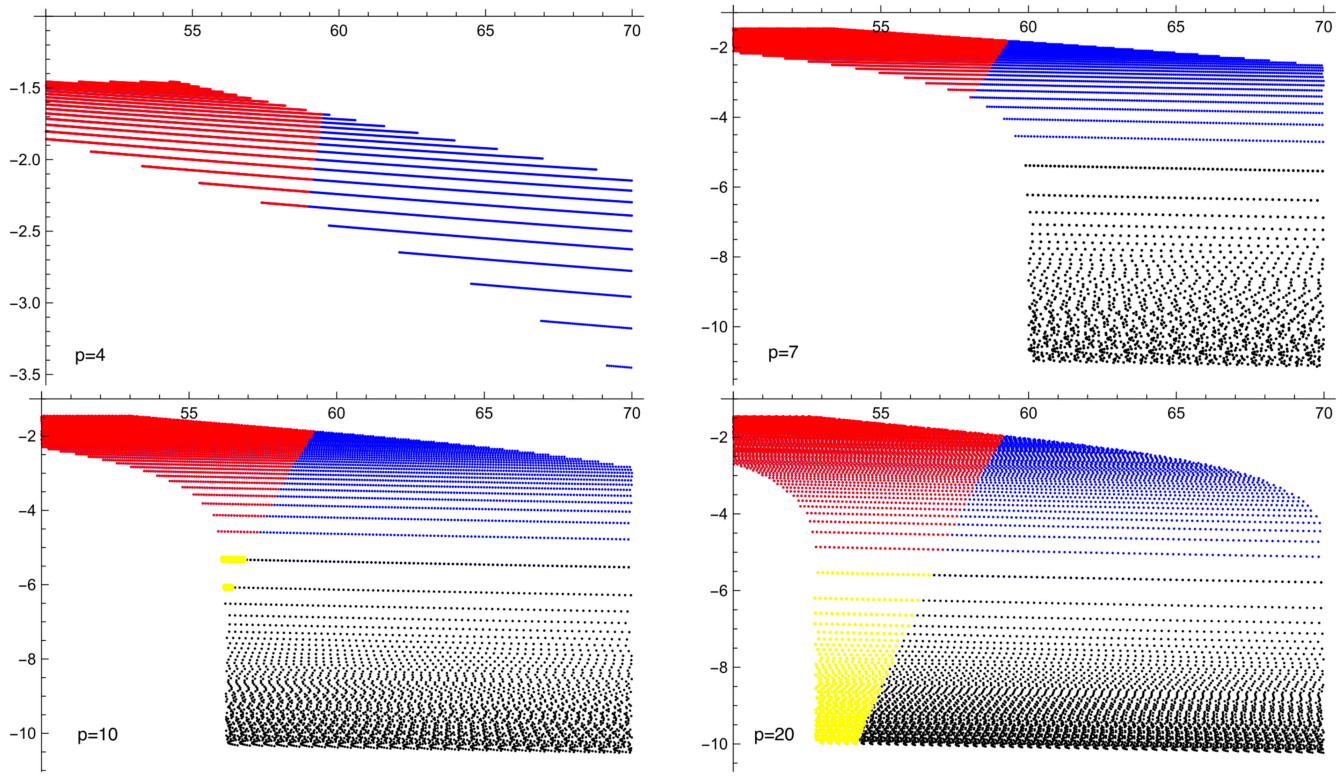

FIG. 3. The tensor ratio distribution $(N_*, \log r)$ for $p = 4, 7, 10, 20$. The color scheme and the arrangement is as in Fig. 1.

Making sufficiently strong approximations to yield analytical methods leads to a loss of significant features. To gain a broader perspective of scaling in inflation, we analyze the scaling behavior of hilltop inflation for both the spectral tilt δ_n and the tensor ratio r as functions of the number of e-folds. We extend this analysis for a wide range of models and a large range of μ values that have been shown in the previous section to be viable [see, e.g., the distributions of the viable μ data in the $(n_{\mathcal{RR}}, r)$ plane for different p shown in Fig. 1].

In Fig. 2 we collect the distributions for $\delta_n(N,\mu)$ as p increases and μ is varied over its viable range. The results show that δ_n scales with N in dependence of the energy scale μ

$$\delta_n(N,\mu) = \frac{\alpha_{\delta_n}(\mu)}{N^{\beta_{\delta_n}(\mu)}}, \tag{18}$$

where the existence of families of the energy-dependent exponents extends the limit defined by the strong small-field approximation SF.III with its energy-independent scaling exponent. Figure 2 shows again that the range of viable e-folds is dramatically affected by the reheating constraint.

It was noted in the previous section that there is a weak correlation between the energy scale μ and the number of inflationary e-folds N_*. In Fig. 2 this degeneracy can be seen explicitly for the different models and that the distribution does become more narrow as p increases.

In Fig. 3 we show the scaling distributions of the tensor-to-scalar ratio $r(N,\mu)$ as p and μ are varied on a logarithmic scale. The resulting behavior

$$r(N,\mu) = \frac{\alpha_r(\mu)}{N^{\beta_r(\mu)}} \tag{19}$$

again shows an energy dependence of the exponents that goes beyond the small-field approximation.

The gap at low r and low N in the graphs of Fig. 3 is quite pronounced for small p, but becomes smaller as p increases. This pattern continues for $p > 20$. Furthermore, the viable regions including the reheating constraint increase, in particular, for the sub-Planckian range of μ.

The two scaling relations (18) and (19) of Figs. 2 and 3 explain the scaling relations in Fig. 1, leading to a nonlinear relation between the spectral tilt and the tensor ratio. They also explain the scaling behavior of the number of reheating e-folds and the reheating temperature as functions of the spectral tilt δ_n or the tensor ratio r. This will be analyzed quantitatively in the next section.

VI. SCALING EXPONENTS IN HILLTOP INFLATION

In this section, we make the scaling behavior of the spectral tilt and the tensor ratio of the hilltop potentials more precise. In Figs. 1–3 the scaling behavior of $r(\delta_n)$, $\delta_n(N)$, and $r(N)$ is shown for several hilltop models in a systematic way for the full super-Planckian range of μ values as well as a partial range of sub-Planckian values. The resulting stratifications in these distributions suggest a scaling behavior of the form $\delta_n(N) = \alpha_\delta N^{-\beta_\delta}$ and $r(N) = \alpha_r N^{-\beta_r}$, with exponents β and amplitudes α that depend on the energy scale μ. Hence we obtain for a given model a family of exponents for each of these observables. This is qualitatively similar to the multifield behavior considered in [42]. In the present discussion, we will determine the resulting exponents β explicitly in order to be able to compare these characteristic numbers of hilltop inflation with those of other models and place this class in the inflationary landscape. The results below can be compared to the small μ limit of the small-field approximation prediction

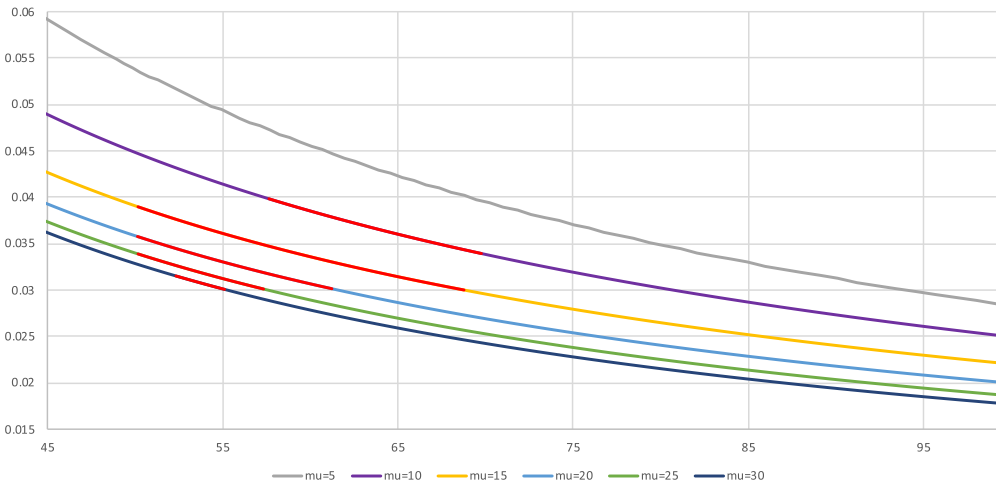

FIG. 4. Scaling behavior of the spectral tilt (N_*, δ_n) for the selection of μ of Table I. Here the red sections along the curves cover the range that is compatible with the CMB and the e-fold constraints.

TABLE I. Characteristic exponents $\beta_{\delta_n}(\mu)$ for the spectral tilt $\delta_n(N)$ in the quartic hilltop model.

μ	5	10	15	20	25	30
$\beta_{\delta_n}(\mu)$	0.924	0.838	0.833	0.86	0.886	0.906

TABLE II. The scaling exponents of the tensor ratio $r(N)$ at $p = 4$.

$\mu/M_{\rm Pl}$	5	10	15	20	25	30
$\beta_r(\mu)$	2.748	2.268	1.897	1.667	1.532	1.446

where both exponents are constants for a fixed model. In the slow-roll approximation these families of exponents instead lead to a nontrivial functional behavior.

A. Scaling exponents for the quartic hilltop model

As noted above, the hilltop model at $p = 4$ has been discussed extensively in the literature, see, e.g., [2,9–12,16,24–26,29,30,32,33], and has been adopted as a benchmark model by the CMB collaborations (see, e.g., [3,4,7]). We therefore begin our analysis with this model for the most general range of μ. In the previous section, we have seen that this model leads to viable initial values compatible with the CMB results only for super-Planckian μ values in a fairly narrow range. As a consequence, parts of the analyses of some of the earlier references are no longer applicable.

The distribution in the spectral-tensor plane is shown in the previous section in Fig. 1, both with and without the reheating constraint. In the present discussion we focus on the scaling behavior of the observables as functions of N. Figure 2 illustrates again that the spectral tilt $\delta_n = 1 - n_{\mathcal{RR}}$ of the spectral index away from the Harrison-Zeldovich spectrum $n_{\mathcal{RR}} = 1$ shows for the quartic hilltop model scaling behavior in dependence of the inflationary e-fold number N_* as indicated above in Eq. (18). In Fig. 4 we make this scaling relation more explicit for several curves describing $\delta_n(N)$ for the hilltop model at $p = 4$.

The curves in Fig. 4 lead to the exponents collected in Table I.

The results of Fig. 4 and Table I show an energy-dependent scaling exponent $\beta_{\delta_n}(\mu)$, which for small μ approaches the limiting value of the SF.III approximation, given by $\beta_{\delta_n} = 1$, while the amplitude is in this limit given by $2(p-1)/(p-2) = 3$. Roughly speaking, the slow-roll approximation leads to a scaling behavior for $p = 4$ hilltop of the form $\delta_n(N) \sim N^{-0.8*}$ in the μ range indicated in Table I.

For the tensor ratio r the first panel in Fig. 3 shows a similar power-law scaling behavior $r(N) = \alpha_r N^{-\beta_r}$ for the quartic hilltop model and a similar analysis leads to scaling functions that for a selection of μ scales are illustrated in Fig. 5.

The scaling exponents β_r associated with the curves of $r(N)$ in Fig. 5 lead to the results in Table II.

This can be compared to the analytical tensor ratio scaling behavior obtained in the SF.III approximation. In this approximation the scaling exponent β_r is independent of μ and its value is given by $\beta_r^{\rm III} = 2(p-1)/(p-2) = 3$. The above results show the μ dependence of the scaling exponents $\beta_r(\mu)$ and that for small μ they approach the value of the strong small-field approximation SF.III.

With the scaling relations $\delta_n(N)$ and $r(N)$ determined above, we can also eliminate N in the second by using the tilt scaling to obtain a scaling relation of the form $r = r(\delta_n)$. The resulting exponents β_r and β_{δ_n} can be compared with the analytical scaling relation determined in the SF.II approximation in Eq. (11). Alternatively, one can analyze the distributions of Fig. 1 directly in the same way as done above for the N-scaling functions. This places

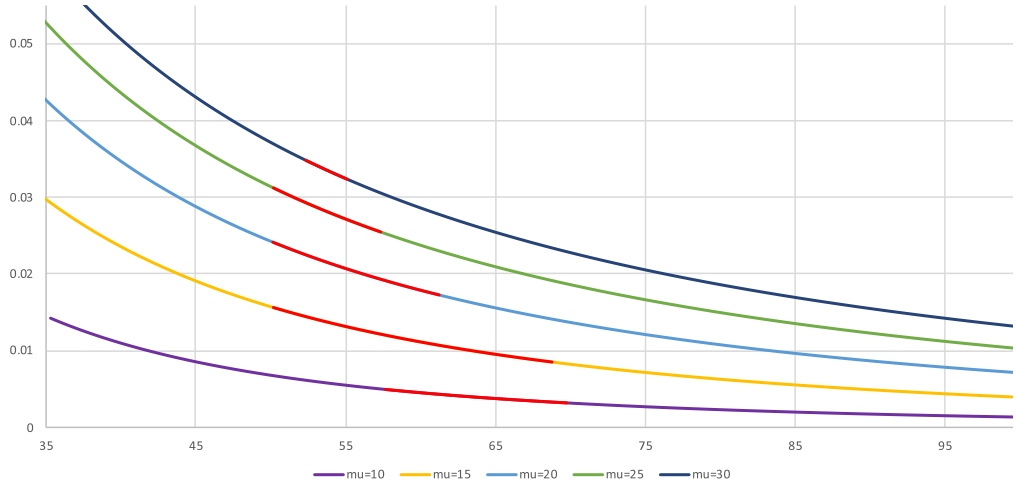

FIG. 5. Scaling behavior of the tensor ratio (N_*, r) for quartic hilltop inflation.

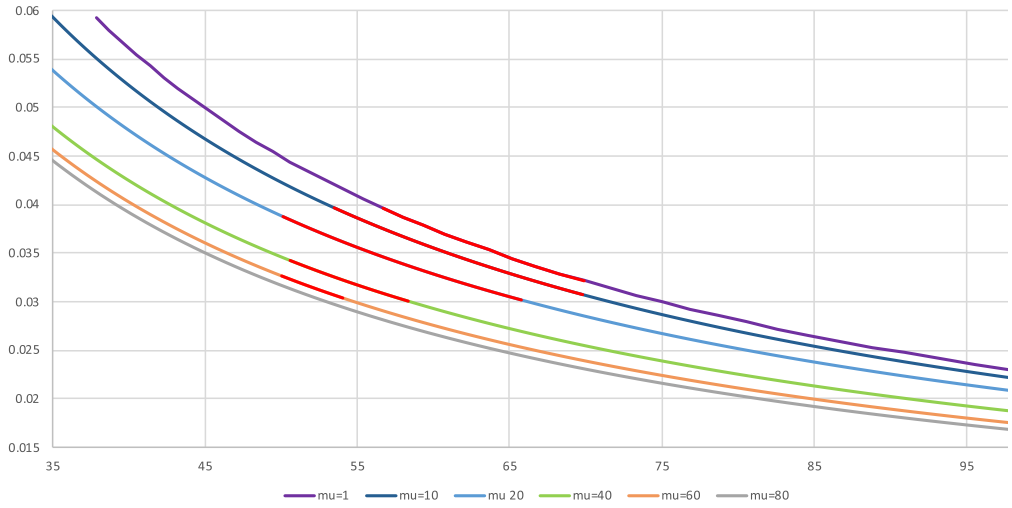

FIG. 6. Scaling behavior of (N_*, δ_n) for $p = 10$ hilltop inflation.

$r(\delta_n)$ directly in spectral-tensor plane and with a measurement of r would allow tests not only of the model but also of the parameter space spanned by μ.

The postinflationary evolution constraint is illustrated in this paper with a matter dominated reheating phase. The implications of the reheating constraint for the different models are shown in the first three figures for both the super-Planckian and the sub-Planckian energy scales μ. For hilltop inflation with $p = 4$ the reheating e-fold range is with our run parameters roughly $\Delta N_{\rm rh} = 40$, while the reheating temperature $T_{\rm rh}$ is roughly between 10^3 and 10^{15} GeV.

B. Behavior of hilltop inflation at $p = 10$

For $p \geq 5$ the range of viable energies μ includes the sub-Planckian regime. In the present section we briefly summarize here the scaling results at $p = 10$, which are obtained in the same way as described in detail in the previous subsection for $p = 4$. For this model the sub-Planckian values for the energy scale μ lead to a much deeper range for the tensor ratio.

The distribution (δ_n, N) for all viable initial values at $p = 10$ takes the form shown in Fig. 2. Similar to the case $p = 4$, the distribution at $p = 10$ is again formed by a set of curves [that are described by a scaling relation in dependence of μ of the type in Eq. (19)]. The scaling curves for a selection of energy scales μ are collected in Fig. 6.

The scaling exponents for the curves in Fig. 6 can be found in Table III. The values obtained can again be compared to those of the small-field approximation, where the amplitude evaluates for $p = 10$ to $\alpha_{10} = 9/4$.

TABLE III. Scaling exponents β_p for δ_n in hilltop inflation at $p = 10$.

$\mu/M_{\rm Pl}$	1	20	40	60	80
$\beta_{\delta_n}(\mu)$	0.998	0.922	0.916	0.934	0.947

We consider again the behavior of the tensor-to-scalar ratio r, for which Fig. 7 shows the dependence on the inflationary number of e-folds for $r(N_*)$ for several energy values μ extracted from the distribution of μ-family curves in Fig. 3.

The scaling curves in Fig. 7 lead to the scaling exponents compiled in Table IV. These results can again be compared to the analytical tensor ratio scaling behavior that can be obtained in the SF.III approximation. The latter predicts that $\beta_r^{\rm III} = 2.25$.

The reheating parameters $N_{\rm rh}$ and $T_{\rm rh}$ for the $p = 10$ hilltop model are comparable to the values for the quartic hilltop model.

As the exponent p of the hilltop models increases, the pattern of the distributions in Fig. 1 is stable in that the spectral-tensor plane region that is viable under CMB + e-fold constraints remains saturated as for the $p = 20$ model. Furthermore, the range of the scaling exponents decreases and remains within the viable region for larger ranges for the energy scale μ.

The above results for the hilltop models at $p = 4$ and $p = 10$ already indicate that these two inflationary scenarios can be characterized by the ranges they define for the scaling exponents of the spectral tilt and the tensor ratio. This will be discussed in more detail in Sec. IX, after the analysis of the hilltop-squared models.

C. Implications

The energy dependence of the N-scaling behavior of any observable

$$\mathcal{O}(N) = \alpha_{\mathcal{O}} N^{-\beta_{\mathcal{O}}} \tag{20}$$

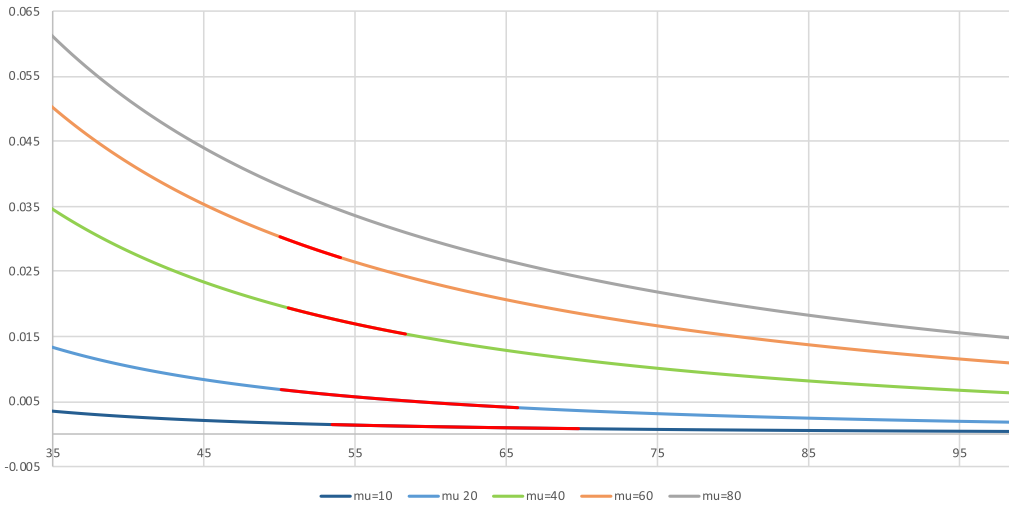

FIG. 7. Scaling behavior of (r, N_*) at $p = 10$.

can be used to determine how the uncertainties of parameters describing the inflationary and reheating phases are affected by varying μ. Denoting these parameters by $\mathcal{P}$, for example, the e-folds of the inflationary and reheating phases, and the reheating temperature, their uncertainty is determined by the uncertainties $\Delta\mathcal{O}$ associated with either the measured values of $\mathcal{O}$ or the uncertainties of fiducial values predicted for future experiments. By inverting (20) the induced uncertainty of the inflationary number of e-folds is determined by

$$\Delta N = -\frac{\alpha_{\mathcal{O}}^{1/\beta_{\mathcal{O}}}}{\beta_{\mathcal{O}}} \frac{\Delta\mathcal{O}}{\mathcal{O}^{1+\frac{1}{\beta_{\mathcal{O}}}}}, \tag{21}$$

which depends on μ via the energy dependence of the amplitude $\alpha_{\mathcal{O}}(\mu)$ and the exponent $\beta_{\mathcal{O}}(\mu)$. This in turn can be used to trace the implications of the uncertainties of $\mathcal{O}$ for $\Delta T_{\rm rh}$. To do so it is useful to make the dependence of $T_{\rm rh}$ on the number of inflationary e-folds explicit by writing Eq. (17) for the reheating temperature via Eq. (15) for the number of reheating e-folds as

$$T_{\rm rh} = \kappa F(\phi_*) \exp\left(\frac{3(1+w_{\rm rh})}{(1-3w_{\rm rh})} N_*\right), \tag{22}$$

where

TABLE IV. The scaling exponents of $r(N)$ for $p = 10$ hilltop inflation.

$\mu/M_{\rm Pl}$	1	20	40	60	80
$\beta_r(\mu)$	2.24	1.92	1.62	1.46	1.37

$$F(\phi_*) = \left(\frac{f_*^{3w_{\rm rh}}}{(f'_*)^{1+3w_{\rm rh}}}\right)^{1/(1-3w_{\rm rh})} \tag{23}$$

and κ collects all the remaining terms that are independent of ϕ_* and N_*. With these ingredients we obtain

$$\frac{\Delta T_{\rm rh}}{T_{\rm rh}} = \left(\frac{3(1+w_{\rm rh})}{1-3w_{\rm rh}} + \frac{F'_*}{F_*}\right)\Delta N_*, \tag{24}$$

where here the dimensionless derivative is relative to the number of e-folds $F' = dF/dN$. The energy dependence of the scaling amplitude $\alpha_{\mathcal{O}}(\mu)$ and the exponent $\beta_{\mathcal{O}}(\mu)$ therefore leads to a μ dependence of these uncertainties. Using, for example, the estimates of the CMB-S4 and the Simons collaborations [5–7] this leads to uncertainties induced by the spectral index and the tensor ratio.

VII. BIFURCATION AMONG p-FAMILIES IN HILLTOP INFLATION

In the previous sections we have analyzed the behavior of the spectral tilt δ_n and the tensor-to-scalar ratio r of hilltop models in dependence of model parameters p and μ, as well as the number of e-folds N, leading to functions on the theory space. Our strategy has been to consider a wide range of models and determine the energy ranges that are compatible with the constraints provided by the CMB data and the e-fold constraints. This leads to energy-dependent scaling exponents that we interpret as diagnostic tools to characterize inflationary models.

An alternative view of the class hilltop models can be obtained by varying the models systematically by letting p run while keeping μ and N_* fixed, leading to a p-family. By subsequently varying μ we obtain a set of p-families in the spectral-tensor plane, as shown in Fig. 8. The strategy here is to determine ϕ_e in the slow-roll approximation as the

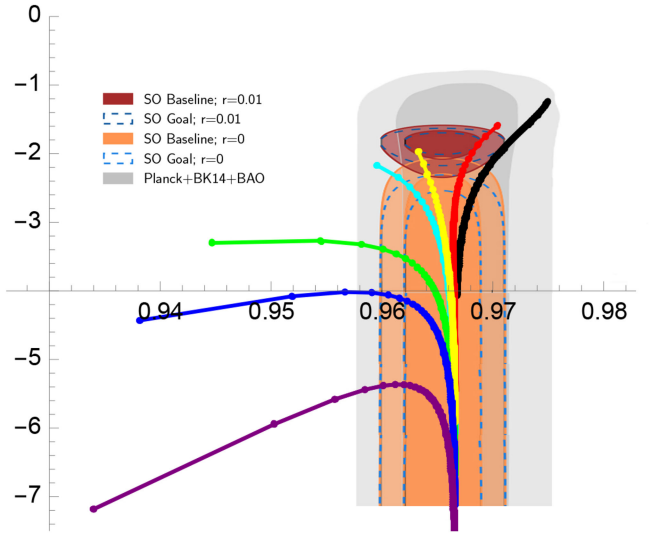

FIG. 8. A selection of p-families in the $(n_{\mathcal{RR}}, \log r)$ plane for different energy scale $\mu/M_{\rm Pl}$ values between 1 (purple, low left corner) and 100 (in black, upper right corner). The forecasts here are by the Simons Observatory (SO) Collaboration [5] for different scenarios.

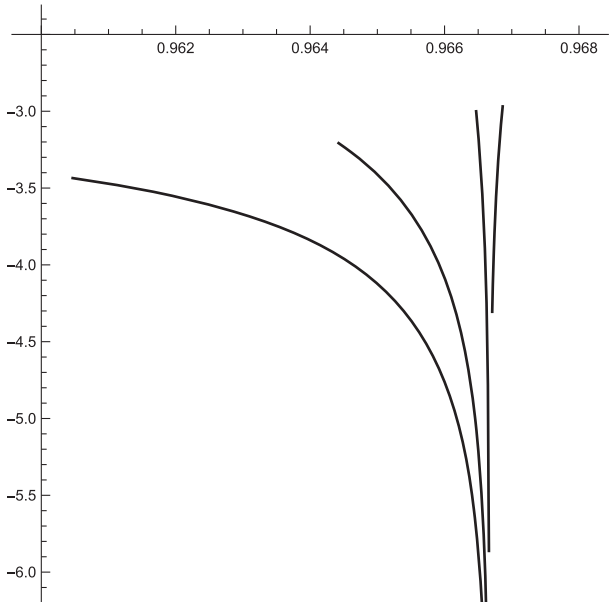

FIG. 9. An illustration of the SF.II approximation of the bifurcation phenomenon in the $(n_{\mathcal{RR}}, \log r)$ plane for hilltop inflation with energy scales between $5M_{\rm Pl}$ and 100 $M_{\rm Pl}$ with p running for $p > p_\mu$, where p_μ is the consistency bound.

solution of the degree p constraint of Eq. (5) and to determine $\phi_*(N, p)$ via Eq. (6). This type of analysis gives further insight into the differences between the hilltop models and it also illustrates the energy dependence of the observables described earlier in this paper in a different way.

A. The bifurcation phenomenon for p-families

Naively, one might have expected that as μ increases the p-family curve becomes ever steeper in the spectral-tensor plane, perhaps approaching the vertical line. This turns out not to be the case. Instead, when changing the μ parameter we find that at some "critical value" μ_c a bifurcation arises in the plane spanned by the spectral index and the tensor ratio. For low μ the trajectories begin at low $n_{\mathcal{RR}}$ for low p values, with increasing $n_{\mathcal{RR}}$ as p increases. Beyond the critical value of μ the p-families begin for small p at large $n_{\mathcal{RR}}$, with decreasing $n_{\mathcal{RR}}$ as p increases. This is illustrated in Fig. 8, which also contains an overlay of the forecasts of the Simons Observatory to illustrate how different models are affected by experimental constraints. The precise location of the bifurcation in the plane depends on the choice of the e-folds. In a first approximation this location is clear from the approximation of the spectral index in the form of Eq. (12), which ignores the ϕ_e dependence of the e-folds. In this approximation the large p-limit approaches the spectral index $n_{\mathcal{RR}} = 1\text{–}2/N_*$.

The structure of the p-families in Fig. 8 illustrates in a different way the results of the scan analysis earlier in this paper, in particular, the fact that for any super-Planckian energy scale μ there are hilltop models that are compatible with the CMB and lead to sufficient inflation. It also illustrates that for low p-models there is a cutoff in the super-Planckian regime below which no viable models can be found. This includes, in particular, the quartic model for which sub-Planckian energy is ruled out.

B. Small-field structure of p-families

It is clear that the bifurcation of the p-families in the spectral-tensor plane cannot be understood in the approximation of hilltop inflation in which the dependence of the number of e-folds on the field ϕ_e at the end of inflation is neglected. This approximation leads to the spectral index (12) and the tensor ratio (13) considered in the early literature [9–11]. The reason why the ϕ_e-terms have often been neglected is because the focus was on the low range of the energy scale μ, in which case the N-independent terms in the denominators of the small-field approximation are small and it is justified to neglect them. An unusual feature of this procedure is that the spectral index does not depend on the energy scale. While it is usually the case that $n_{\mathcal{RR}}$ does not depend on the overall energy scale Λ, it does, in general, depend on the remaining parameters of the theory, and we see here that in the less severe SF.II approximation this is also the case for hilltop inflation.

To illustrate that the SF.II approximation does capture the bifurcation, we consider in Fig. 9 several p-family curves in this approximation for several μ values between 1 and 200 $M_{\rm Pl}$. This graph is truncated compared to the numerical slow-roll graph in Fig. 8 because of the p-dependent consistency constraints on the energy scale μ in this approximation. Nevertheless, it does show that the

bifurcation phenomenon can be captured by the SF.II approximation even though the detailed numerics of the trajectories is, of course, different in pure slow-roll as compared to the SF.II approximation.

VIII. HILLTOP-SQUARED INFLATION

We have noted already that hilltop inflation $V_{p,n}$ as defined in Eq. (1) with $n = 1$ does not contain a minimum valley in which the inflaton can oscillate during reheating. While this is, in principle, easy to fix with a small deformation of the potential close to its zero, this feature has motivated the consideration of more global changes of the hilltop models, such as hilltop-squared inflation (HSI), with potentials of the type considered in Eq. (1) with $n = 2$ [23]. Higher exponents n have been considered in [26,32,34,35].

In the present section, we extend our analysis of the scaling behavior of the spectral tilt and the tensor ratio considered above for hilltop inflation (HI) to potentials of the type

$$V_{p,2} = \Lambda^4\left(1 - \left(\frac{\phi}{\mu}\right)^p\right)^2. \tag{25}$$

We focus, in particular, on the phenomenological aspects and the scaling behavior of these models. We find that the scaling results for the hilltop-squared models differ from those of the hilltop models, but that they follow a similar overall pattern.

A. Observables in hilltop-squared inflation

The spectral index of the scalar perturbations for the hilltop-squared inflationary models (25) is given by

$$n_{\mathcal{RR}}^{\mathrm{HSI}} = 1 - \frac{4p\frac{M_{\mathrm{Pl}}^2}{\mu^2}}{(1-(\frac{\phi}{\mu})^p)^2}\left(\frac{\phi}{\mu}\right)^{p-2}\left[(p-1)+(p+1)\left(\frac{\phi}{\mu}\right)^p\right] \tag{26}$$

and the tensor ratio r^{HSI} relates to the hilltop tensor ratio as

$$r^{\mathrm{HSI}}(\phi) = 32p^2\frac{M_{\mathrm{Pl}}^2}{\mu^2}\frac{(\frac{\phi}{\mu})^{2(p-1)}}{(1-(\frac{\phi}{\mu})^p)^2} = 4r. \tag{27}$$

The inflaton field at the end of inflation ϕ_e is determined in HSI_p by

$$x_e^p + \sqrt{2}p\frac{M_{\mathrm{Pl}}}{\mu}x_e^{p-1} - 1 = 0, \tag{28}$$

where $x_e = \phi_e/\mu$. The number of e-folds N_*^{HSI} is related to that of hilltop inflation as

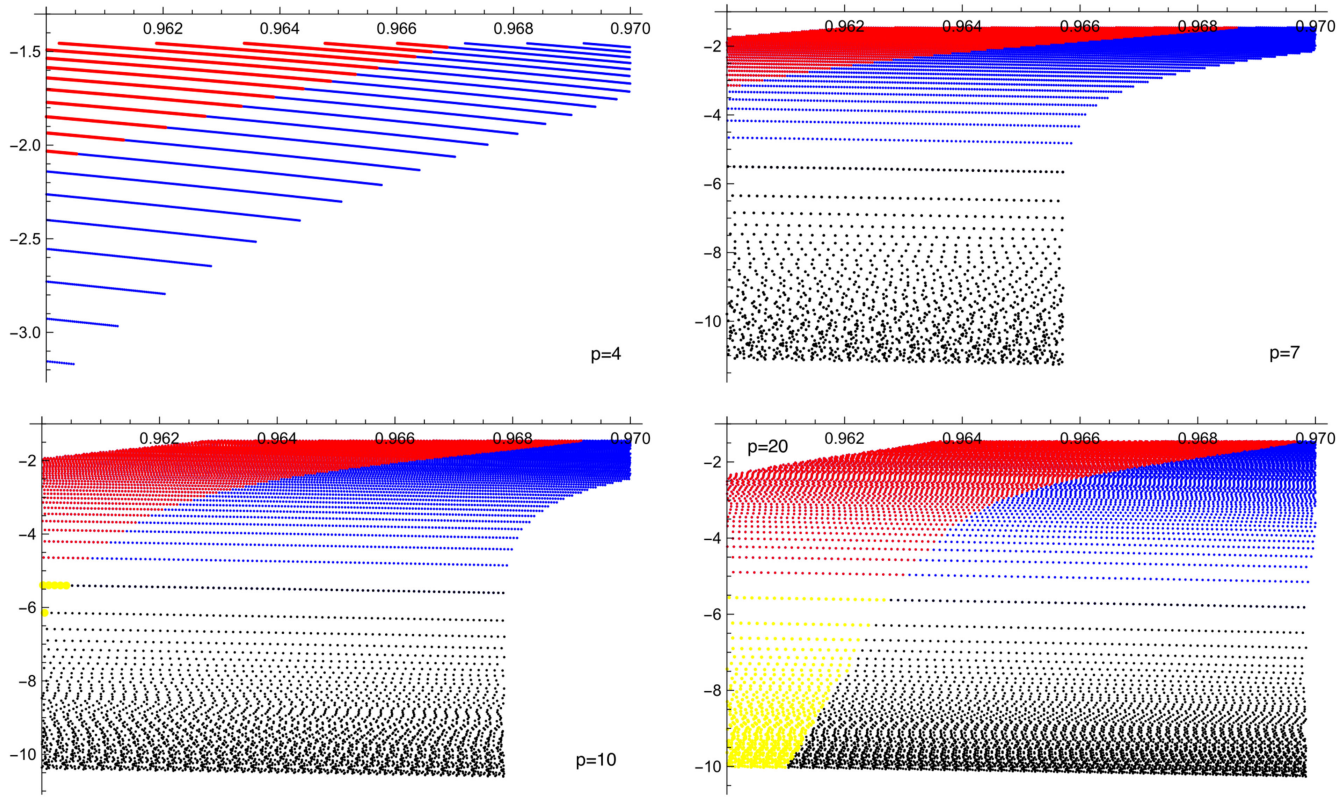

FIG. 10. The spectral-tensor distributions $(n_{\mathcal{RR}}, \log r)$ for hilltop-squared models with $p = 4, 7, 10, 20$. The color scheme is the same as in Fig. 1. For $p = 4$, 7 the reheating constraint rules out sub-Planckian μ.

$$N_*^{\mathrm{HSI}} = \frac{1}{2} N_*^{\mathrm{HI}}. \tag{29}$$

The reheating e-fold number N_{rh} and the reheating temperature T_{rh} can be obtained from the general formulas given above in (15) and (17) via the dimensionless hilltop-squared potential.

B. Distribution of $(r, n_{\mathcal{RR}})$ in hilltop-squared inflation

In the present subsection, we consider a sample of HSI_p models for the same range of p values considered above for hilltop inflation and with the same CMB and reheating constraints so as to be consistent with the PLANCK results for the observables. The number of e-folds is again in the canonical interval [50, 70]. Figure 10 shows the distribution in the spectral-tensor plane.

These results imply that hilltop-squared inflation is not small-field inflation, in general, in the sense that for some p models sub-Planckian field values are not compatible with the CMB constraints. This is similar to the behavior of the hilltop models discussed above. The panel in Fig. 10 for hilltop-squared at $p = 4$ shows, in particular, that the allowed range in the spectral-tensor plane is quite small and that there are, in particular, no sub-Planckian energies μ that lead to viable initial values. One can check that this implies that the inflaton values ϕ_* for this model are all super-Planckian and hence hilltop-squared inflation at $p = 4$ is not small-field inflation. The same holds for the $p = 3$ model.

C. Scaling distributions for hilltop-squared observables via N

The behavior of the spectral tilt δ_n is of interest both from a theoretical and a practical perspective, as discussed above in the context of the hilltop models. Figure 11 shows the scaling distributions for the spectral tilt δ_n for different p models in hilltop-squared inflation. Like in hilltop inflation these distributions show a weak correlation between the energy scales μ and the number of inflationary e-folds.

D. $r(N)$ scaling in hilltop-squared inflation

The behavior of the tensor-to-scalar ratio r as a function of the number of inflationary e-folds N_* in hilltop-squared inflation is similar to that of hilltop inflation. Figure 12 illustrates the $(N, \log 4)$-scaling relations for several hilltop models. As in the case of the hilltop models, the viable region for $p = 4$ is much smaller than that of the higher p models.

E. Scaling exponents in hilltop-squared inflation

The analysis of the scaling behavior in hilltop-squared inflation follows the same strategy as in hilltop inflation.

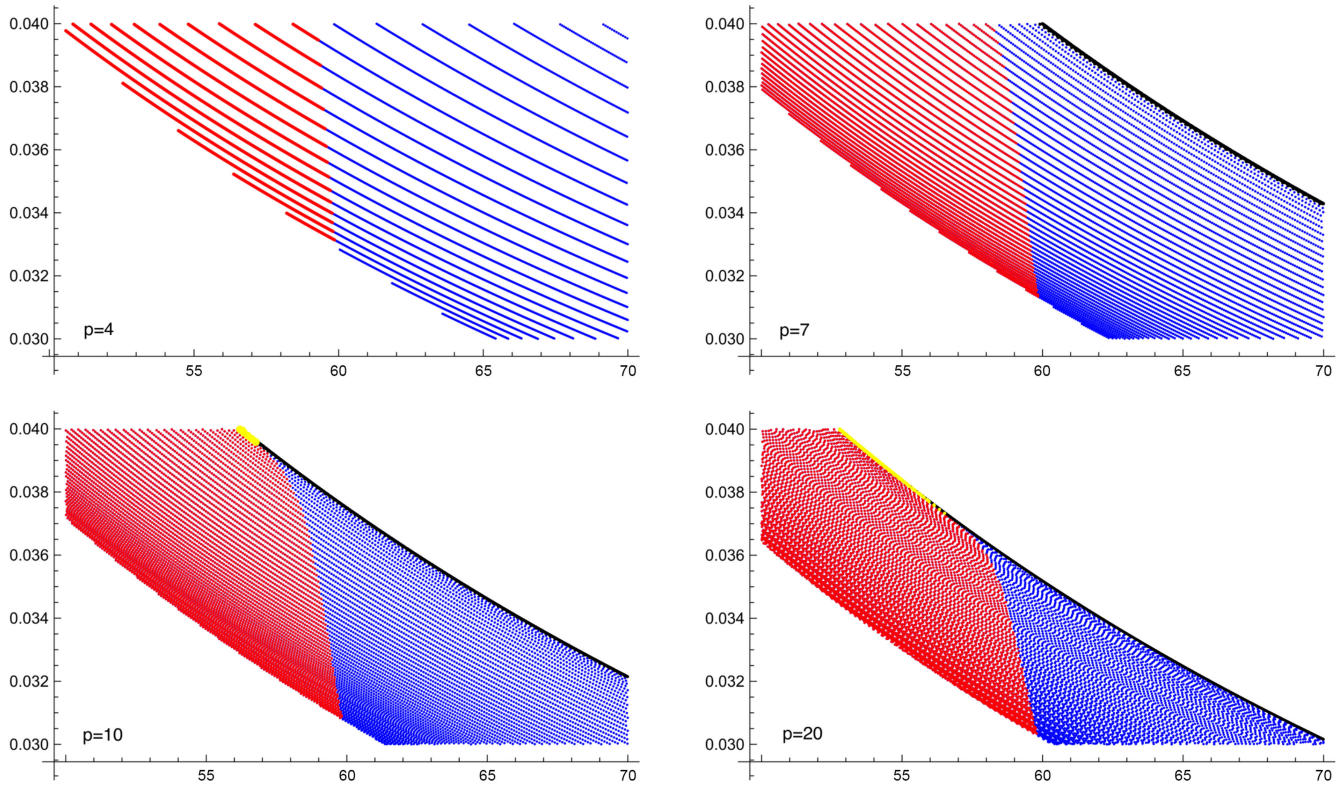

FIG. 11. The (N_*, δ_n) distributions for hilltop-squared models $p = 4, 7, 10, 20$. The color coding is the same as in Fig. 1. For $p = 4$ there are no contributions from sub-Planckian μ, hence there are no black and yellow regions in the corresponding panel.

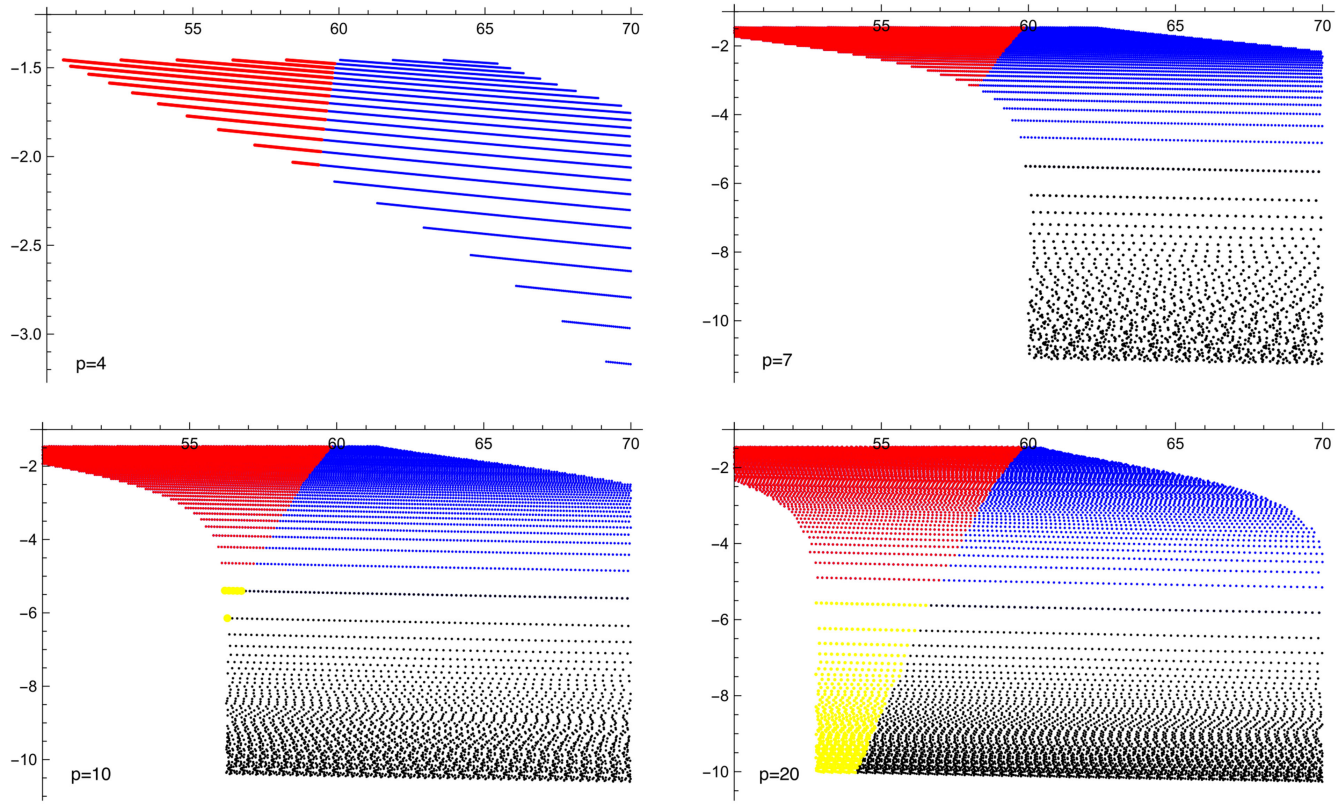

FIG. 12. Distributions of $(N_*, \log r)$ for hilltop-squared models at $p = 4$, 7, 10, 20. The color scheme is the same as in Fig. 1.

The structure of the two classes of models is similar, although the numerical results differ. We have analyzed a wide range of models between $p = 3$ and $p = 100$, based on the distributions discussed in the previous sections and extensions thereof, but here we focus on the $p = 4$ hilltop-squared model to illustrate the results. The distribution in the spectral-tensor plane shown in Fig. 12 establishes the regions that are viable given the CMB inflationary constraints with or without the reheating constraint. In the following we focus on the scaling exponents of the tensor ratio in dependence of the number of e-folds, shown for several models in Fig. 12 as a function of the energy scale μ. Some aspects of this model other than scaling have also been discussed in [32]. In Fig. 13 we select several curves from the distribution shown in the $p = 4$ panel of Fig. 12.

The scaling exponents for the curves in Fig. 13 lead to the results listed in Table V.

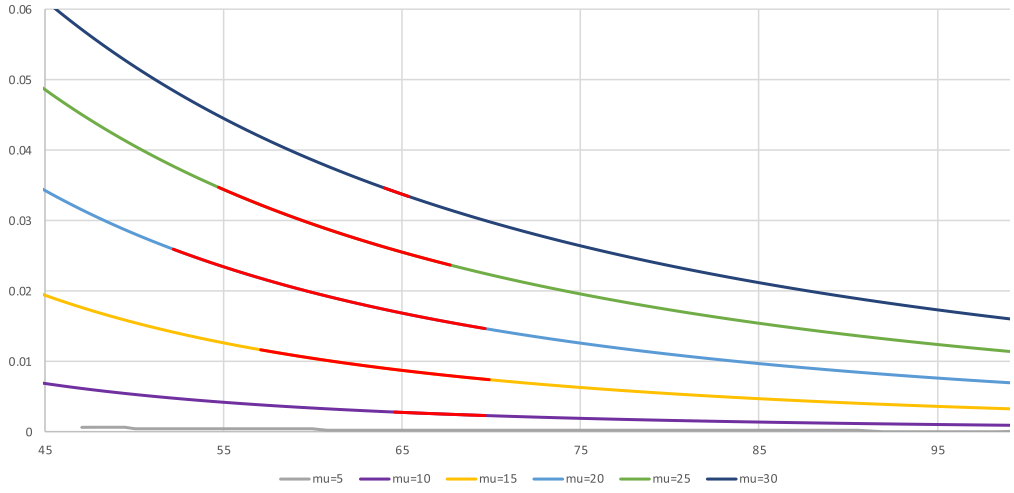

FIG. 13. A selection of (N_*, r) curves for hilltop-squared inflation at $p = 4$.

TABLE V. Scaling exponents $\beta_r(\mu)$ for at $p = 4$ HSI.

μ	5	10	20	25	30
$\beta_r(\mu)$	2.859	2.546	1.958	1.798	1.687

For hilltop-squared models, the range of the scaling exponents becomes more narrow as p increases because the upper boundary decreases and the lower boundary changes only slightly.

IX. SCALING EXPONENTS AS MODEL CHARACTERISTICS

In the previous sections we have determined the scaling exponents of the two main observables $n_{\mathcal{RR}}, r$ as functions of the number of inflationary e-folds in both hilltop and hilltop-squared inflationary models. These power-law scaling exponents depend on the energy parameter μ of the models, leading for a given model to functions $\beta_\delta(\mu)$ and $\beta_r(\mu)$. More generally, we can think of observables $\mathcal{O}(N)$ and their associated exponents $\beta_\mathcal{O}(\mu)$ as functions on the model parameter space. These energy scales are constrained, depending on the conditions imposed on the observables. If one is interested in what present and future experiments can observe, then these constraints include those obtained from CMB and large scale survey data, assumptions about the number of inflationary e-folds N_* and, in principle, assumptions about the reheating period and other constraints. Given such a set of μ-dependent scaling exponents for an observable $\mathcal{O}$ it is natural to ask how they characterize different models. The discussion above suggests that this can be achieved in different ways. An immediate comparison of models can be obtained by comparing the ranges of the exponents for different models, leading to what we will call "characteristic intervals." A second way is to focus on the functional form of the scaling exponents, leading to "characteristic functions."

A. Characteristic intervals

One possibility to distinguish different inflationary models in an observable-based way is by comparing the characteristic intervals obtained by imposing the CMB constraints and the number of inflationary e-folds. The results above of the analyses of hilltop and hilltop-squared inflation show that for both types of models the strong small-field approximation SF.III leads to an upper bound of the corresponding characteristic intervals. For small p this upper limit is quite different from the actual upper limit, but for larger p the energy-independent SF.III exponent $\beta_r^{\mathrm{III}} = 2(p-1)/(p-2)$ is quite close to the slow-roll upper bound of the tensor ratio scaling $r(N)$.

In order to gain perspective, it is useful to compare the hilltop and hilltop-squared results above with results obtained in other models. In Ref. [42] a scaling analysis of the type considered in the present paper was constructed for two modular inflationary models, theories that are based on softly broken groups $\mathrm{SL}(2,\mathbb{R})$, associated with a hyperbolic target space. In these models the potentials are invariant under discrete subgroups of the Möbius group and the theories have two energy scales (Λ, μ), much like the hilltop and hilltop-squared families. The observables $n_{\mathcal{RR}}$ and r can be viewed as functions of the number of e-folds and show scaling behavior that is also energy dependent. The resulting exponents again sweep out characteristic intervals and hence can be compared with the results obtained in the present paper. The fact that the β_r^{III} define the upper limit for the energy-dependent exponents immediately implies that the hilltop and hilltop-squared models define scaling classes that are distinct from the scaling classes defined by modular inflationary models considered in [42] because the characteristic intervals of hilltop and hilltop-squared inflation have no overlap with the models considered there. This shows that characteristic intervals provide a useful diagnostic for both single-field and two-field inflation.

The comparison of the characteristic intervals of the two hilltop classes, on the other hand, shows that they are similar, with a somewhat higher lower bound of $\beta_r(\mu)$ for hilltop-squared models as compared to hilltop models. Roughly speaking, the distribution of these values in the hilltop-squared class is more narrow than in hilltop inflation.

B. Characteristic functions of scaling exponents

A second defining feature that can be considered, once the distribution of the scaling exponents $\beta_\mathcal{O}(\mu)$ of an observable $\mathcal{O}$ is known, is their functional form. Here we focus on the tensor-to-scalar ratio for hilltop and hilltop-squared inflation, similar to the analysis considered for modular inflation in Ref. [42]. In both HI and HSI inflation it is tempting to use as a guide for the functional fit the fact that for large p the exponents $\beta(\mu)$ are approximately flat because for large p these models behave similar to the strong small-field approximation SF.III and in this approximation there is no μ dependence. This suggests a linear ansatz for the $\beta(\mu)$ as a comparison to the horizontal line determined by SF.III. It turns out, however, that this is not a good approximation, in general, as seen already earlier in the analyses above.

We make the functional μ dependence of the tensor scaling exponents explicit in Fig. 14 for the classes of hilltop and hilltop-squared inflation for six different models between $p = 3$ and $p = 100$ and an energy range $\mu \leq 150 M_{\mathrm{Pl}}$. The gray bands indicate the characteristic intervals of the approximate range of exponents for which the models are compatible with the CMB and e-fold constraints. For small p these μ have a lower bound that is super-Planckian, hence for these models the exponent functions leave this CMB region at smaller values of μ and again for larger μ, depending on p. For larger p the μ range

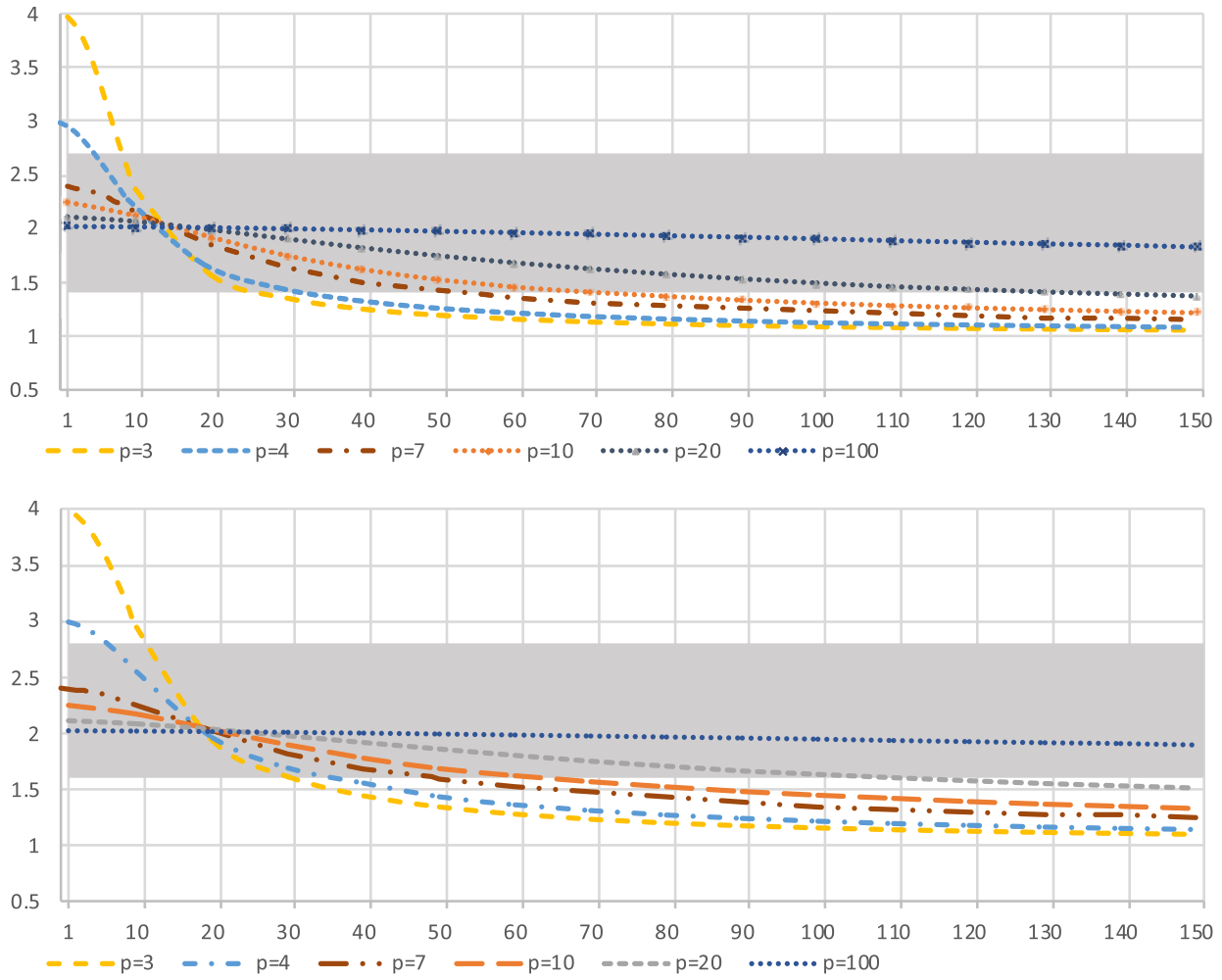

FIG. 14. The functional dependence of the scaling exponents β_r (vertical axis) of the tensor ratio $r(N)$ on the energy scale μ (horizontal axis) at $p = 3, 4, 7, 10, 20, 100$ for hilltop (top) and hilltop-squared inflation (lower). The gray region indicates the values for which the different models are compatible with the CMB and e-fold based constraints.

reaches down quite far into the sub-Planckian regime and the functional form of scaling exponents $\beta_r(\mu)$ becomes flatter as the viable μ range expands. It is only for the largest p models considered here that the exponents remain completely within the characteristic band in the whole range of μ considered in the graphs.

The behavior of the $r(N)$ exponents in Fig. 14 for hilltop and hilltop-squared models shows that for the complete range of μ values, irrespective of the precise observational constraints, the functions $\beta_r(\mu)$ can be described by higher degree polynomials for low p, with the degrees decreasing as the model exponents p increase. These polynomial fits for $\beta_r(\mu)$ thus provide intrinsic characteristic functions of the models. In the parameter ranges that are viable relative to the CMB and e-fold constraints, the functions $\beta_r(\mu)$ become simpler in the sense that fewer parameters suffice for a good description.

The results obtained here for hilltop and hilltop-squared inflation can now be compared with the results obtained in [42] for modular inflationary models. For those models the μ range was restricted to the super-Planckian range $\mu > 10M_{\rm Pl}$ and the models showed a simple scaling-of-scaling behavior with exponents δ_r that were very similar, both close to $\delta_r \cong 2$. In order to compare the hilltop models to these modular inflationary models, it is useful to restrict them to the same energy range. This leads again to an approximate simple scaling behavior with exponents δ_r in dependence of p. These hilltop scaling exponents are much smaller than 2, establishing that the resulting scaling-of-scaling behavior can be used as a classification tool that distinguishes between these two different classes of models. The advantage of this analysis is that a single numerical exponent allows one to characterize a model and its parameter space.

X. CONCLUSIONS

In this paper we have shown how the energy-dependent scaling exponents $\beta_{\mathcal{O}}(\mu)$ associated with observables $\mathcal{O}(N)$

as functions of the number N of inflationary e-folds can be used to characterize the classes of hilltop and hilltop-squared inflation. Our focus has been on the spectral tilt δ_n and the tensor-to-scalar ratio r, leading to an analysis of the behavior of the scaling exponents $\beta_{\delta_n}(\mu)$ and $\beta_r(\mu)$ of $\delta_n(N)$ and $r(N)$. Here the energy scale μ is constrained by the conditions imposed, which include the CMB and the e-fold constraint, but may also include other restrictions, for example, the reheating constraint. In the classes of hilltop and hilltop-squared inflation these constraints lead to μ ranges that increase as the exponent p is increased, leading to increasing domains of functions $\beta_{\mathcal{O}}$. The resulting scaling exponents $\beta_r(\mu)$ then lead to two different modes in which models can be classified, first via their characteristic intervals and second via the functional types of the scaling exponents.

The scaling results for the hilltop and hilltop-squared models for $\beta_{\mathcal{O}}(\mu)$ are quite similar, as expected, indicating that the differences seen by the inflaton toward the end of inflation do not lead to significant changes in the present context. The behavior of these two classes is, however, quite different from that of the modular inflationary models considered in [42]. Using the characteristic interval as a diagnostic tool shows that the modular inflationary models are quite distinct from hilltop inflation and hilltop-squared inflation since the tensor exponents of the former have no overlap with the tensor exponents of the latter. Hence these models belong to different regions of the inflationary landscape. The functional behavior of hilltop and hilltop-squared models is also quite similar, but again quite different from that of the modular models. Comparing modular inflation with hilltop/hilltop-squared inflation shows that the CMB + e-fold compatible range of μ for hilltop and hilltop-squared inflation is much larger than for the modular inflationary models. As discussed in Sec. IX, for the full viable range the functional behavior of the exponents depends quite dramatically on the model parameter p. In order to compare HI and HSI models with modular inflation, it is necessary to restrict the energy scale to about $\mu \geq 10M_{\rm Pl}$. In this range the functional behavior of HI and HSI simplifies and can be approximated as a power-law scaling relation, leading to different inflationary scaling regimes.

An immediate implication of the energy dependence of the scaling exponents of both $\delta_n(N)$ and $r(N)$ is that this leads to an energy-dependent scaling behavior for $r(\delta_n)$, leading to a family of curves in the spectral-tensor plane. This will have consequences for the type of reheating analysis considered for example in [58].

The fact that hilltop and hilltop-squared models lead to scaling regimes that are different from that of the modular inflation models considered in [42] raises the question whether the scaling diagnostics considered here generalize to other models. It would be interesting to place other inflationary models in the scaling framework considered here, either for single-field inflationary models or for theories with more than one inflaton field. Analyzing models such as those considered in the single-field encyclopedia [2], or multifield models, including, for example, the models considered in Refs. [59–71], will provide further insight into the scaling structure of the inflationary landscape.

ACKNOWLEDGMENTS

It is a pleasure to thank Ali Ishaq and Vipul Periwal for discussions and correspondence. This work was supported in part by a sabbatical leave of absence.

[1] D. H. Lyth and A. Riotto, Particle physics models of inflation and the cosmological density perturbations, Phys. Rep. **314**, 1 (1999).
[2] J. Martin, C. Ringeval, and V. Vennin, Encyclopedia inflationaris, Phys. Dark Universe **5**, 75 (2014).
[3] P. Ade *et al.* (Planck Collaboration), Planck 2015 results. XX. Constraints on inflation, Astron. Astrophys. **594**, A20 (2016).
[4] Y. Akrami *et al.* (Planck Collaboration), Planck 2018 results, X, Inflation, Astron. Astrophys. **641**, A10 (2020).
[5] P. Ade *et al.* (Simons Observatory Collaboration), The Simons Observatory: Science goals and forecasts, J. Cosmol. Astropart. Phys. 02 (2019) 056.
[6] K. N. Abazajian *et al.* (CMB-S4 Collaboration), CMB-S4 Science book, first edition, arXiv:1610.02743.
[7] K. Abazajian *et al.* (CMB-S4 Collaboration), CMB-S4 Science case, reference design and project plan, arXiv:1907.04473.
[8] P. A. R. Ade *et al.* (BICEP/Keck Collaboration), Improved constraints on primordial gravitational waves using Planck, WMAP, and BICEP/Keck observations through the 2018 observational season, Phys. Rev. Lett. **127**, 151301 (2021).
[9] W. H. Kinney and K. T. Mahanthappa, Inflation from symmetry breaking below the Planck scale, Phys. Lett. B **383**, 24 (1996).
[10] W. H. Kinney and K. T. Mahanthappa, Inflation at low scales: General analysis and a detailed model, Phys. Rev. D **53**, 1533 (1996).
[11] D. H. Lyth, What would we learn by detecting a gravitational wave signal in the CMB anisotropy?, Phys. Rev. Lett. **78**, 1861 (1996).

[12] L. Boubekeur and D. Lyth, Hilltop inflation, J. Cosmol. Astropart. Phys. 07 (2005) 010.
[13] W. H. Kinney and A. Riotto, Theoretical uncertainties in inflationary predictions, J. Cosmol. Astropart. Phys. 03 (2006) 011.
[14] J. Martin and C. Ringeval, Inflation after WMAP3: Confronting the slow-roll and exact power spectra with CMB data, J. Cosmol. Astropart. Phys. 08 (2006) 009.
[15] K. Kohri, C.-M. Lin, and D. H. Lyth, More hilltop models, J. Cosmol. Astropart. Phys. 12 (2007) 004.
[16] S. Bird, H. V. Peiris, and R. Easther, Fine-tuning criteria for inflation and the search for gravitational waves, Phys. Rev. D **78**, 083518 (2008).
[17] J. Martin and C. Ringeval, First CMB constraints on inflationary reheating temperature, Phys. Rev. D **82**, 023511 (2010).
[18] P. Adshead, R. Easther, J. Pritchard, and A. Loeb, Inflation and the scale dependent spectral index: Prospects and strategies, J. Cosmol. Astropart. Phys. 02 (2011) 021.
[19] R. Easther and H. V. Peiris, Bayesian analysis of inflation II: Model selection and constraints on reheating, Phys. Rev. D **85**, 103533 (2012).
[20] D. Roest, Universality classes of inflation, J. Cosmol. Astropart. Phys. 01 (2014) 007.
[21] J. Garcia-Bellido and D. Roest, The large-N running of the spectral index of inflation, Phys. Rev. D **89**, 103547 (2014).
[22] G. Barenboim, W.-I. Park, and W. H. Kinney, Eternal hilltop inflation, J. Cosmol. Astropart. Phys. 05 (2016) 030.
[23] V. Domcke, M. Pieroni, and P. Binetruy, Primordial gravitational waves for universality classes of pseudoscalar inflation, J. Cosmol. Astropart. Phys. 06 (2016) 031.
[24] C.-M. Lin, Type I hilltop inflation and the refined swampland criteria, Phys. Rev. D **99**, 023519 (2019).
[25] D. Chowdhury, J. Martin, C. Ringeval, and V. Vennin, Inflation after Planck: Judgement day, Phys. Rev. D **100**, 083537 (2019).
[26] R. Kallosh and A. Linde, On hilltop and brane inflation after Planck, J. Cosmol. Astropart. Phys. 09 (2019) 030.
[27] R. Goswami and U. A. Yajnik, Reheating constraints to modulus mass for single field inflationary models, Nucl. Phys. **B960**, 115211 (2020).
[28] P. Adshead, J. T. Giblin, M. Pieroni, and Z. J. Weiner, Constraining axion inflation with gravitational waves from preheating, Phys. Rev. D **101**, 083534 (2020).
[29] K. Dimopoulos, An analytic treatment of quartic hilltop inflation, Phys. Lett. B **809**, 135688 (2020).
[30] G. German, Quartic hilltop inflation revisited, J. Cosmol. Astropart. Phys. 02 (2021) 034.
[31] C. Osses, N. Videla, and G. Panotopoulos, Reheating in small-field inflation on the brane: The swampland criteria and observational constraints of the Planck 2018 results, Eur. Phys. J. C **82**, 485 (2021).
[32] J. Hoffmann and D. Sloan, Squared quartic hilltop inflation, Phys. Rev. D **104**, 123542 (2021).
[33] J. L. Cook, Primordial black hole production in natural and hilltop inflation, J. Cosmol. Astropart. Phys. 07 (2023) 031.
[34] H. G. Lillepalu and A. Racioppi, Generalized hilltop inflation, Eur. Phys. J. Plus **138**, 894 (2023).
[35] A. Ghoshal, M. Y. Khlopov, Z. Lalak, and S. Porey, Post-inflationary production of particle dark matter: Hilltop and Coleman-Weinberg inflation, Phys. Rev. D **109**, 063037 (2024).
[36] R. Schimmrigk, Automorphic inflation, Phys. Lett. B **748**, 376 (2015).
[37] R. Schimmrigk, A general framework for automorphic inflation, J. High Energy Phys. 05 (2016) 140.
[38] R. Schimmrigk, Modular inflation observables and j-inflation phenomenology, J. High Energy Phys. 09 (2017) 043.
[39] R. Schimmrigk, Multifield reheating after modular j-inflation, Phys. Lett. B **782**, 193 (2017).
[40] M. Lynker and R. Schimmrigk, Modular inflation at higher level N, J. Cosmol. Astropart. Phys. 06 (2019) 036.
[41] R. Schimmrigk, Large and small field inflation from hyperbolic sigma models, Phys. Rev. D **105**, 063541 (2022).
[42] M. Lynker and R. Schimmrigk, Scaling behavior of observables as a model characteristic in multifield inflation, J. Cosmol. Astropart. Phys. 04 (2023) 039.
[43] G. German, G. G. Ross, and S. Sarkar, Low-scale inflation, Nucl. Phys. **B608**, 423 (2001).
[44] R. Armillis and C. Pallis, Implementing hilltop F-term hybrid inflation in supergravity, in *Recent Advances in Cosmology*, edited by A. Traverna and B. Soren (Nova Science Publishers, 2013), arXiv:1211.4011.
[45] R. Armillis, G. Lazarides, and C. Pallis, Inflation, leptogenesis and Yukawa quasiunification within a supersymmetric left-right model, Phys. Rev. D **89**, 065032 (2014).
[46] V. N. Lukash, Production of sound waves in the early universe, Pi'sma Zh. Eksp. Teor. Fiz. **31**, 631 (1980) [JETP Lett. **31**, 596 (1980)].
[47] J. M. Bardeen, Gauge-invariant cosmological perturbations, Phys. Rev. D **22**, 1882 (1980).
[48] S. Weinberg, *Cosmology* (Oxford University Press, New York, 2008).
[49] L. Dai, M. Kamionkowski, and J. Wang, Reheating constraints to inflationary models, Phys. Rev. Lett. **113**, 041302 (2014).
[50] J. B. Munoz and M. Kamionkowski, Equation-of-state parameter for reheating, Phys. Rev. D **91**, 043521 (2015).
[51] J.-O. Gong, G. Leung, and S. Pi, Probing reheating with primordial spectrum, J. Cosmol. Astropart. Phys. 05 (2015) 027.
[52] R.-C. Cai, Z.-K. Guo, and S.-J. Wang, Reheating phase diagram for single-field slow-roll inflationary models, Phys. Rev. D **92**, 063506 (2015).
[53] J. L. Cook, E. Dimastrogiovanni, D. A. Easson, and L. M. Krauss, Reheating predictions in single field inflation, J. Cosmol. Astropart. Phys. 04 (2015) 047.
[54] E. Allys *et al.* (LiteBIRD Collaboration), Probing cosmic inflation with the LiteBIRD CMB polarization survey, Prog. Theor. Exp. Phys. **2023**, 042F01 (2023).
[55] T. Sprenger, M. Archidiacono, T. Brinckmann, S. Clesse, and J. Lesgourgues, Cosmology in the era of Euclid and the square kilometer array, J. Cosmol. Astropart. Phys. 02 (2019) 047.
[56] J.-Q. Jiang, G. Ye, and Y.-S. Piao, Return of Harrison-Zeldovich spectrum in light of recent cosmological tensions, Mon. Not. R. Astron. Soc. **527**, L54 (2023).
[57] W. Giarè, F. Renzi, O. Mena, E. Di Valentino, and A. Melchiorri, Is the Harrison-Zeldovich spectrum coming back? ACT preference for $n_s \sim 1$ and its discordance with Planck, Mon. Not. R. Astron. Soc. **521**, 2911 (2023).

[58] M. Drewes and L. Ming, Connecting cosmic inflation to particle physics with LiteBIRD, CMB S4, Euclid and SKA, arXiv:2208.07609.
[59] A. Linde, Hybrid inflation, Phys. Rev. D **49**, 748 (1994).
[60] T. Higaki and F. Takahashi, Elliptic inflation: Interpolation from natural inflation to R^2 inflation, J. High Energy Phys. 03 (2015) 129.
[61] S. Mizuno and S. Mukohyama, Primordial perturbations from inflation with a hyperbolic field-space, Phys. Rev. D **96**, 103533 (2017).
[62] S. Mizuno, S. Mukohyama, S. Pi, and Y.-L. Zhang, Hyperbolic field space and swampland conjecture for DBI scalar, J. Cosmol. Astropart. Phys. 09 (2019) 072.
[63] L. Anguelova, E. M. Babalic, and C. I. Lazaroiu, Hidden symmetries of two-field cosmological models, J. High Energy Phys. 09 (2019) 007.
[64] V. Aragam, S. Paban, and R. Rosati, Multi-field inflation in high-slope potentials, J. Cosmol. Astropart. Phys. 04 (2020) 022.
[65] F. Carta, N. Righi, Y. Welling, and A. Westphal, Harmonic hybrid inflation, J. High Energy Phys. 12 (2020) 161.
[66] K. Kogai and Y. Tada, Escape from the swamp with spectator, Phys. Rev. D **101**, 103514 (2020).
[67] E. M. Babalic and C. I. Lazaroiu, The infrared behavior of tame two-field cosmological models, Nucl. Phys. **B983**, 115929 (2022).
[68] C. I. Lazaroiu, Natural coordinates and horizontal approximations in two-field cosmological models, arXiv:2305.12547.
[69] Y. Abe, T. Higaki, F. Kaneko, T. Kobayashi, and H. Otsuka, Moduli inflation from modular flavor symmetry, J. High Energy Phys. 06 (2023) 187.
[70] R. Krishnan, Symmetries of stationary points of the G-invariant potential and the framework of the auxiliary group, Phys. Rev. D **103**, L051701 (2021).
[71] R. Krishnan, Homogeneous linear intrinsic constraints in the stationary manifold of a G-invariant potential, arXiv:2306.07325.